Magnetism in Solids _____

A numerical method to determine demagnetization factors of stadium-shaped nanoislands for artificial spin ices

Victoria Martinez¹ and Ezio Iacocca¹

¹ Center for Magnetism and Magnetic Nanostructures, University of Colorado Colorado Springs, Colorado Springs, CO 80918, USA

Received xxxx 00, 0000, revised xxxx 00, 0000, published xxxx 00, 0000, current version xxxx 00, 0000 (Dates will be inserted by IEEE; "published" is the date the accepted preprint is posted on IEEE Xplore[®]; "current version" is the date the typeset version is posted on Xplore[®]).

Abstract—The shape of nanoislands gives rise to a demagnetizing field that is primarily responsible for the orientation of the magnetization along an axis. In the context of magnetization dynamics, the demagnetization field also determines the resonant frequencies captured by Kittel's equations. Analytically, we require demagnetization (demag) factors that can be obtained exactly for a few geometries, including ellipsoids and prisms. However, analytical expressions are not available for other shapes, limiting the use of Kittel equation as a predictive model. Here, we present a method to obtain the demag factors from micromagnetic simulations with good accuracy. Similar to experiments, we obtain ferromagnetic resonance but we use orthogonal field conditions to fit Kittel equation unambiguously and obtain the demag factors with good accuracy. This method will be useful to determine demag factors under the ellipsoidal approximation for stadium-shaped nanoislands used in artificial spin ices (ASIs) and thus lead to better prediction in their ferromagnetic resonance and band structures.

Index Terms— Magnetism in Solids, nanoislandics.

I. INTRODUCTION

Artificial spin ices (ASIs) are geometric arrays of nanoislands that exhibit vastly degenerate states [Skjærvø 2020]. As magnonic crystals [Gliga 2020, Lendinez 2019], ASIs have been proposed as reconfigurable metamaterials with tunable band structure [Iacocca 2016], controllable FMR spectra [Jungfleisch 2016, Dion 2019, Arroo 2019, Iacocca 2020, Gartside 2021, Negrello 2022], evidence of topological bands [Iacocca 2017], and application in unconventional computing [Caravelli 2023, Caravelli 2022, Gartside 2022]. The potential use of ASIs relies on the dipolar coupling between individual elements and its impact on the resulting FMR frequencies and band structure. For this reason, it is of practical interest to provide an accurate analytical determination of the FMR frequency. For example, a recent approach [Alatteili 2023] is able to compute FMR for generalized ASI geometries using a minimal analytical model.

Because ASIs are typically studied with no or weak applied fields, the FMR frequency is sensitive to the demagnetization field of the individual magnetic nanoislands [Bahl 2021]. Because the magnetic nanoislands are in a monodomain state, it is analytically desirable to utilize the ellipsoidal approximation [Osborn 1945] for the magnetometric demag factors [Chen 1991]. However, the magnetic nanoislands are typically shaped as stadia, leading to quantitative differences between experiments and simple application of Kittel's equation [Kittel 1948]. Therefore, the demag factors must be adjusted to reproduce Kittel's equation under the ellipsoidal approximation, i.e., when the demag tensor is diagonal [Aharoni 2001].

Corresponding author: Ezio Iaccoca (eiacocca@uccs.edu). Digital Object Identifier 10.1109/LMAG.2020.Doi Number Here, we fit Kittel's equation to determine effective demag factors for stadium-shaped nanoislands and compare it with the analytical demag factors for the general ellipsoid [Osborn 1945] and the rectangular prism [Aharoni 1998]. We use micromagnetic simulations to obtain the FMR response of stadium-shaped nanoislands, but the same method could be used for experimental data. However, micromagnetic simulations allow to explore a range of nanoislands sizes with ease and thus obtain formulas to predict the nonlinear dependence of demag factors in order to explore the FMR response of ASIs with a variety of nanoisland sizes and arrangements. In other words, the goal of the method presented here is to obtain demag factors that can be used to analytically predict features in the FMR response of general ASIs based on the FMR response of individual nanoislands. Both micromagnetic and processing scripts are publicly available [OSF].

II. Methodology

A. Micromagnetic FMR response

FMR is traditionally obtained by detecting the absorption spectrum of a magnet when either an external field or a microwave field's frequency are varied. Numerically, this process is time consuming, so alternatives are often sought [Wagner 2021, d'Aquino 2022]. Here, we used a pulsed excitation to determine the resonances of nanoislands in a numerically efficient manner [Iacocca 2016, Iacocca 2017]. Micromagnetic simulations were performed using the Mumax3 package [Vansteenkiste 2014]. We used a uniform 10 ps field pulse of magnitude 10 mT to tilt the magnetization and record the magnetization's average dynamic relaxation. This technique has been previously used to compare with experiments [Jungfleisch 2016, Lendinez 2023]. The simulation ran for 20 ns and the data was saved every $\delta t = 2.5$ ps. We also use zero-padding to

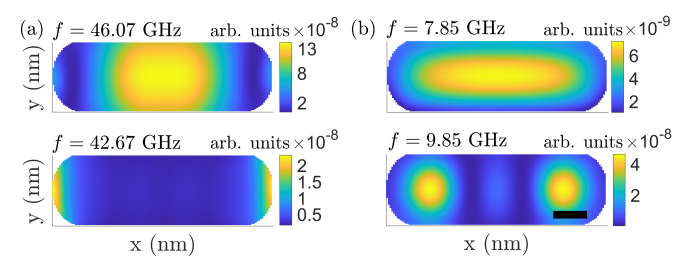


Fig. 1. Mode profiles of a stadium-shaped nanoisland. The modes were obtained by magnetizing nanoisland in the (a) easy axis, x direction and (b) hard axis, z direction. In (a), we used an external field of $\mu_0 H_x = 1.1$ T. The bulk and edge mode are shown in the top and bottom row, at 46.07 GHz and 42.67 GHz respectively . In (b), we used an external field of $\mu_0 H_z = 1.2$ T. The bulk and higher-order mode are shown in the top and bottom row, at 7.85 GHz and 9.85 GHz respectively. The scale bar in panel (b) is $15\,\mathrm{nm}$.

reduce the frequency resolution to 4 MHz while keeping a maximum resolved frequency of 200 GHz. It is important to apply the pulse orthogonal to the saturating field, so that a net torque is applied to the system without incurring in nonlinearities, i.e., parametric pumping. This method excites all quantized modes in the nanoislands from which the bulk mode more closely aligns with the FMR mode [Gliga 2013].

To determine the bulk mode, we first investigated the spatial profile of the excited modes. For example, in Fig. 1 we show the mode profiles for a stadium-shaped nanoisland of dimensions $125 \text{ nm} \times 50 \text{ nm} \times 5 \text{ nm}$. The stadium-shaped nanoislands are generated in Mumax3 by combining a rectangular section of dimension 75 nm \times 50 nm \times 10 nm and two circular regions with diameter 50 nm appended to the edges of the rectangular region, such that the caps of the nanoislands are semicircles. For all simulations, we used the material parameters for permalloy: $M_s = 790 \text{ kA/m}$, A = 10 pJ/m and $\alpha = 0.01$. The magnetocrystalline anisotropy was neglected. In panel (a), the nanoisland was magnetized along the easy x axis and external field of $\mu_0 H_x = 1.1$ T was used. The mode profile in the top panel at f = 46.07 GHz is a bulk mode, spanning most of the available volume. The mode profile in the bottom panel at f = 42.67 GHz is an edge mode. In panel (b) we show the mode profiles for the nanoisland magnetized along the hard z axis with an external field of $\mu_0 H_z = 1.2$ T. The bulk mode is observed at f = 7.85 GHz, shown in the top row, occupying virtually all the available volume. The mode at f = 9.85 GHz is a higher-order mode. We use the bulk mode as an approximation of FMR in nanoislands in the remainder of the paper.

B. Fitting procedure with Kittel's equation

From the micromagnetic simulations, we obtain the field-dependent frequency of the bulk modes. Because we need to fit three quantities, \mathcal{N}_x , \mathcal{N}_y , and \mathcal{N}_z , we need three simultaneous equations. For this, we utilize the field-dependent frequency of the bulk modes when an external field is applied along the easy and hard axes. We

then fit the system of equations

$$\begin{array}{lcl} \frac{\omega}{\gamma\mu_0} & = & \sqrt{[H_x+(\mathcal{N}_y-\mathcal{N}_x)M_s][H_x+(\mathcal{N}_z-\mathcal{N}_x)M_s]} \text{(1a)} \\ \frac{\omega}{\gamma\mu_0} & = & \sqrt{[H_z+(\mathcal{N}_y-\mathcal{N}_z)M_s][H_z+(\mathcal{N}_x-\mathcal{N}_z)M_s]} \text{(1b)} \\ 1 & = & \mathcal{N}_x+\mathcal{N}_y+\mathcal{N}_z, \end{array}$$

where Eq. (1c) is included in the fitting procedure to ensure that the demag factors are uniquely determined. We used the Levenberg-Marquardt algorithm to concurrently fit the data with nonlinear least-squares and retrieve both the fitted value and the standard deviation, σ . Because the variables are strongly coupled, the standard deviation is identical for all three demag factors. The standard deviation is defined as $\sigma = \sqrt{\operatorname{diag}\{N(J'J)^{-1}\}}$, where N is the normalized squared residual and J is the Jacobian, both computed during the nonlinear least-square minimization.

III. Results

A. Ellipsoid

To test our method, we simulated an ellipsoid which can be directly compared with the analytical results by J. A. Osborn [Osborne 1945]. The ellipsoid had axes dimensions 200 nm \times 100 nm \times 20 nm discretized in cells of 1.56 nm \times 1.56 nm \times 1.25 nm. This small cell size is used to minimize the errors due to the finite difference method employed in Mumax3 [Iacocca 2017]. In Fig. 2, we show the field-dependent frequency obtained by Mumax3 with red circles when the ellipse was magnetized in the (a) x axis and (b) z axis. From the fits, we computed the field-dependent frequency by Kittel's equation, shown by solid black curves, displaying excellent agreement with the data. In panels (c) and (d) we show the corresponding difference between the frequencies calculated with Kittel equation using the fitted and Osborn demag factors. We find a disagreement of ≈ 1 GHz, which is a relative error of under 0.1 %, but experimentally detectable. The increase of error towards lower fields indicates a disagreement between the numerical and theoretical magnetizing field and it is the main source of error in the computation of demag factors.

The demag factors retrieved are: $\mathcal{N}_x=0.0574\pm0.0361$, $\mathcal{N}_y=0.1503\pm0.0361$, and $\mathcal{N}_z=0.7924\pm0.0361$, to be compared with the analytical solutions [Osborn 1945] $\mathcal{N}_{x,O}=0.0873$, $\mathcal{N}_{y,O}=0.1390$, and $\mathcal{N}_{z,O}=0.7737$. We find that our fitted parameters are all within the standard deviation. Note that, as mentioned above, the standard deviation is identical for all three factors, which reduces the accuracy for the demag factor along the easy axis.

B. Stadium-shaped nanoislands

Having confirmed the validity of our method with ellipsoid nanoislands, we move on to simulate stadium-shaped nanoislands. This shape is created in Mumax3 by Boolean addition of a cuboid and two shifted cylinders. To explore the dependence of the demag factors, we varied the length and width of the nanoislands from 50 nm to 200 nm while keeping the thickness constant at 5 nm.

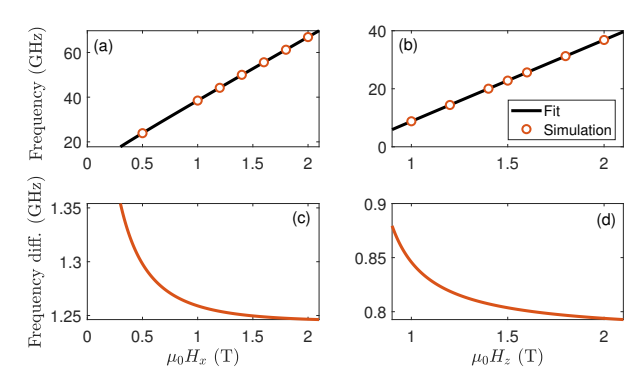


Fig. 2. FMR from micromagnetic simulations (red circles) and fitted Kittel's equations (black curves) for an ellipsoid of dimensions 200 nm \times 100 nm \times 20 nm. The external static field is applied along the (a) z and (b) x axes. The corresponding frequency difference with the prediction from Osborn [Osborn 1945] are shown in (c) and (d), respectively.

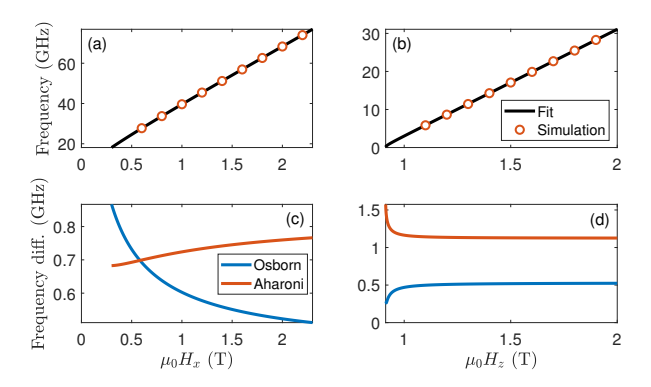


Fig. 3. FMR from micromagnetic simulations (red circles) and fitted Kittel's equations (black curves) for a stadium-shaped nanoisland of dimensions 200 nm \times 100 nm \times 5 nm. The external static field is applied along the (a) z and (b) x axes. The corresponding frequency difference with the prediction from Osborn [Osborn 1945] and Aharoni [Aharoni 1998] are shown in (c) and (d), respectively.

As a proof-of-concept, we show results for stadium-shaped nanosilands of dimensions 200 nm \times 100 nm \times 5 nm in this section. Because the nanoislands are thin, we only use one cell across the thickness, so this is effectively a 2D simulation. The field-dependent frequency and corresponding Kittel equation using the fitted demag factors is shown in Fig. 3(a) and (b). The fitted parameters are $\mathcal{N}_x = 0.0045 \pm 0.0255$, $\mathcal{N}_y = 0.1141 \pm 0.0255$, and $\mathcal{N}_z = 0.8813 \pm 0.0255$. Because of the geometry, we compare with both the prediction from an ellipsoid and a rectangular prism. The analytical values are $\mathcal{N}_{x,O} = 0.0218$, $\mathcal{N}_{y,O} = 0.0347$, and $\mathcal{N}_{z,O}=0.9434$ for the ellipsoid [Osborn 1945] and $\mathcal{N}_{x,A}=$ 0.0315, $\mathcal{N}_{y,A}=0.0647$, and $\mathcal{N}_{z,A}=0.9038$ for the rectangular prism [Aharoni 1998]. We observe that our fitted parameter indicate a lower \mathcal{N}_z factor compared to both ellipsoid and the rectangular prism. The frequency difference between the fits and analytical predictions is shown in Fig. 3(c) and (d). We observe that Aharoni's prediction is better in the in-plane configuration while Osborn's prediction is better in the perpendicular configuration. Our fitted parameters allow us to obtain a good prediction in both cases,

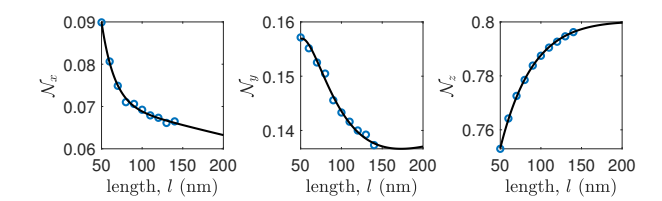


Fig. 4. Empirical fits of the demag factors from 25-nm wide stadia and varying length. The numerically estimated demag factors are show by blue circles and the empirical fits from Eqs. (2) are shown by solid black curves.

especially for small fields that are relevant for artificial spin ices [Dion 2023].

The method was repeated for nanoislands of varying dimensions, with the fitted parameters reported in Table 1. For stadia converging to a perfect circle, it is expected that $\mathcal{N}_z=1$ due to symmetry, and were not numerically computed. However, to approach this value, we computed an approximately circular magnet, from we we obtain $\mathcal{N}_x=0.01829,\,\mathcal{N}_y=0.02795$ and $\mathcal{N}_z=0.95375$.

The method was applied to predict the demag factors for a range of stadia dimensions as an example. These formulas can be then implemented in semi-analytical calculations [Alatteili 2023] to explore certain parameter spaces in the FMR of ASIs. We focused here on stadia of 25 nm in width and varying the length l between 50 nm and 140 nm, i.e., aspect ratios of ≈ 0.36 to 0.5, a range in which we find convergent fits relying in a few data points. Empirical fits can be performed on this data with good accuracy. For the aforementioned stadia, we find empirical fits using the equations

$$\begin{array}{lcl} \mathcal{N}_{z} & \approx & 0.804e^{(-1.567\times10^{-5}~\mathrm{nm}^{-1})l} - 0.169e^{(-0.0245~\mathrm{nm}^{-1})} \mbox{\ensuremath{\rlap/}2a)} \\ \mathcal{N}_{x} & \approx & 0.456e^{(-0.0631~\mathrm{nm}^{-1}))l} + 0.0731e^{(-0.000727~\mathrm{nm}^{-1})l} \mbox{\ensuremath{\rlap/}2b)} \\ \mathcal{N}_{y} & = & 1 - \mathcal{N}_{x} - \mathcal{N}_{z}, \end{array} \tag{2c}$$

shown in Fig. 4. In this case, \mathcal{N}_x and \mathcal{N}_x were used for the fits because it was possible to fit their behavior with double exponential functions. These equations are not general, but can be used to obtain a fast and reliable calculation of demag factors within a certain range of stadia dimensions.

IV. CONCLUSION

We used a numerical method to extract the demag factors for a stadium-shaped nanoisland with good accuracy. The method relies on micromagnetic simulations to simulate FMR and a concurrent fit of Kittel's equations to determine the demag factors. We find demag factors that allow us to accurately recover FMR when nanoislands are subject to in-plane and out-of-plane external fields. This is particularly important to predict FMR at low fields, which is of technological interest in applications and, notably, for artificial spin ices where FMR appears directly as a consequence of the stray fields from nanoislandic arrays. While micromagnetic simulations must be conducted, we show how empirical formulas can be constructed in a range of stadium dimensions. The method is not constrained to stadium-shaped nanoislands, and can in principle be used for any

nanosized ferromagnet. The Mumax3 input file and Matlab script to extract the data and fit the demag factors is available online [OSF].

ACKNOWLEGMENT

V. M. acknowledges the Department of Physics and Energy Science at UCCS for the use of their facilities and equipment. This material is based upon work supported by the National Science Foundation under Grant No. 2205796.

REFERENCES

- A. Aharoni, "Demagnetizing factors for rectangular ferromagnetic prisms," *Journal of Applied Physics*, vol. 83, no. 6, pp. 3432–3434, 1998. [Online]. Available: https://doi.org/10.1063/1.367113
- A. Aharoni, emphIntroduction to the theory of ferromagnetism. Oxford University Press, 2001.
- G. Alatteili, V. Martinez, A. Roxburgh, J. C. Gartside, O. G. Heinonen, S. Gliga, and E. Iacocca, "Gænice: a general model for magnon band structure of artificial spin ices," arXiv:2309.03826. [Online]. Available: https://arxiv.org/abs/2309.03826
- D. M. Arroo, J. C. Gartside, and W. R. Branford, "Sculpting the spin-wave response of artificial spin ice via microstate selection," *Phys. Rev. B*, vol. 100, p. 214425, Dec 2019. [Online]. Available: https://link.aps.org/doi/10.1103/PhysRevB.100.214425
- C. R. H. Bahl, "Estimating the demagnetization factors for regular permanent magnet pieces," AIP Advances, vol. 11, no. 7, p. 075028, 07 2021. [Online]. Available: https://doi.org/10.1063/5.0060897
- F. Caravelli and C. Nisoli, "Logical gates embedding in artificial spin ice," New Journal of Physics, vol. 22, no. 10, p. 103052, 2020. [Online]. Available: https://doi.org/10.1088/1367-2630/abbf21
- F. Caravelli, E. Iacocca, G.-W. Chern, C. Nisoli, and C. I. L. de Araujo, "Anisotropic magnetomemristance," npj Communication Physics, no. 5, p. 166, 2022. [Online]. Available: https://www.nature.com/articles/s42005-022-00942-y
- P. Couture, S. Goldman, R. E. Camley, E. Iacocca, K. L. Livesey, T. Robinson, D. Meyers, S. Maat, H. T. Nembach, and Z. Celinski, "Ferromagnetic resonance of hollow micron-sized magnetic cylinders," *Applied Physics Letters*, vol. 121, no. 20, p. 202403, 2022. [Online]. Available: https://doi.org/10.1063/5.0124550
- M. d'Aquino, C. Serpico, G. Miano, and C. Forestiere, "A novel formulation for the numerical computation of magnetization modes in complex micromagnetic systems," *Journal of Computational Physics*, vol. 228, no. 17, pp. 6130– 6149, 2009. [Online]. Available: https://www.sciencedirect.com/science/article/pii/ S0021999109002642
- T. Dion, D. M. Arroo, K. Yamanoi, T. Kimura, J. C. Gartside, L. F. Cohen, H. Kurebayashi, and W. R. Branford, "Tunable magnetization dynamics in artificial spin ice via shape anisotropy modification," *Phys. Rev. B*, vol. 100, p. 054433, Aug 2019. [Online]. Available: https://link.aps.org/doi/10.1103/PhysRevB.100.054433
- T. Dion, K. D. Stenning, A. Vanstone, H. H. Holder, R. Sultana, G. Alatteili, V. Martinez, M. T. Kaffash, T. Kimura, H. Kurebayashi, W. R. Branford, E. Iacocca, B. M. Jungfleisch, and J. C. Gartside, "Ultrastrong magnon-magnon coupling and chiral symmetry breaking in a 3d magnonic metamaterial," arXiv:2306.16159, 2019.
- J. C. Gartside, A. Vanstone, T. Dion, K. D. Stenning, D. M. Arroo, H. Kurebayashi, and W. R. Branford, "Reconfigurable magnonic mode-hybridisation and spectral control in a bicomponnt artificial spin ice," *Nature Communications*, vol. 12, p. 2488, 2021. [Online]. Available: https://www.nature.com/articles/s41467-021-22723-x
- J. C. Gartside, K. D. Stenning, A. Vanstone, H. H. Holder, D. M. Arroo, T. Dion, F. Caravelli, H. Kurebayashi, and W. R. Branford, "Reconfigurable training and reservoir computing in an artificial spin-vortex ice via spin-wave fingerprinting," *Nature Nanotechnology*, vol. 17, pp. 460–469, 2022. [Online]. Available: https://www.nature.com/articles/s41565-022-01091-7
- M. Getzlaff, Fundamental of magnetism. Springer, 2008.
- S. Gliga, A. Kákay, R. Hertel, and O. G. Heinonen, "Spectral analysis of topological defects in an artificial spin-ice lattice," *Phys. Rev. Lett.*, vol. 110, p. 117205, Mar 2013. [Online]. Available: http://link.aps.org/doi/10.1103/PhysRevLett.110.117205
- S. Gliga, E. Iacocca, and O. G. Heinonen, "Dynamics of reconfigurable artificial spin ice: Toward magnonic functional materials," APL Materials, vol. 8, no. 4, p. 040911, 2020. [Online]. Available: https://doi.org/10.1063/1.5142705
- E. Iacocca, S. Gliga, R. L. Stamps, and O. Heinonen, "Reconfigurable wave band structure of an artificial square ice," *Phys. Rev. B*, vol. 93, p. 134420, Apr 2016. [Online]. Available: http://link.aps.org/doi/10.1103/PhysRevB.93.134420
- E. Iacocca and O. Heinonen, "Topologically nontrivial magnon bands in artificial square spin ices with dzyaloshinskii-moriya interaction," Phys. Rev. Applied,

- vol. 8, p. 034015, Sep 2017. [Online]. Available: https://link.aps.org/doi/10.1103/PhysRevApplied.8.034015
- E. Iacocca, S. Gliga, and O. G. Heinonen, "Tailoring spin-wave channels in a reconfigurable artificial spin ice," *Phys. Rev. Applied*, vol. 13, p. 044047, Apr 2020. [Online]. Available: https://link.aps.org/doi/10.1103/PhysRevApplied.13.044047
- M. B. Jungfleisch, W. Zhang, E. Iacocca, J. Sklenar, J. Ding, W. Jiang, S. Zhang, J. E. Pearson, V. Novosad, J. B. Ketterson, O. Heinonen, and A. Hoffmann, "Dynamic response of an artificial square spin ice," *Phys. Rev. B*, vol. 93, p. 100401, Mar 2016. [Online]. Available: http://link.aps.org/doi/10.1103/PhysRevB.93.100401
- C. Kittel, "On the theory of ferromagnetic resonance absorption," *Phys. Rev.*, vol. 73, no. 2, pp. 155–161, Jan 1948. [Online]. Available: https://journals.aps.org/pr/abstract/10.1103/PhysRev.73.155
- T. D. Lasnier and G. M. Wysin, "Magnetic oscillation modes in square-lattice artificial spin ice," *Phys. Rev. B*, vol. 101, p. 224428, Jun 2020. [Online]. Available: https://link.aps.org/doi/10.1103/PhysRevB.101.224428
- S. Lendinez and M. B. Jungfleisch, "Magnetization dynamics in artificial spin ice," J. Phys.: Condens. Matter, vol. 32, p. 013001, 2019. [Online]. Available: https://iopscience.iop.org/article/10.1088/1361-648X/ab3e78
- S. Lendinez, M. T. Kaffash, O. G. Heinonen, S. Gliga, E. Iacocca, and M. B. Jungfleisch, "Nonlinear multi-magnon scattering in artificial spin ice," *Nature Communications*, vol. 14, p. 3419, 2021. [Online]. Available: https://www.nature.com/articles/s41467-023-38992-7
- R. Negrello, F. Montoncello, M. T. Kaffash, M. B. Jungfleisch, and G. Gubbiotti, "Dynamic coupling and spin-wave dispersions in a magnetic hybrid system made of an artificial spin-ice structure and an extended nife underlayer," APL Materials, vol. 10, no. 9, p. 091115, 2022. [Online]. Available: https://doi.org/10.1063/5.0102571
- J. A. Osborn, "Demagnetizing factors of the general ellipsoid," *Phys. Rev.*, vol. 67, no. 11-12, pp. 351–357, Jun 1945. [Online]. Available: https://journals.aps.org/pr/abstract/10.1103/PhysRev.67.351
- The scripts supporting this research are available at OSF under DOI:10.17605/OSF.IO/YUNHD. [Online]. Available: https://osf.io/yunhd/
- S. H. Skjærvø, C. H. Marrows, R. L. Stamps, and L. J. Heyderman, "Advances in artificial spin ice," *Nat. Rev. Phys.*, vol. 2, pp. 13–28, 2020. [Online]. Available: https://www.nature.com/articles/s42254-019-0118-3
- D. Stancil and A. Prabhakar, Spin waves: Theory and applications. Springer, 2009.
- A. Vansteenkiste, J. Leliaert, M. Dvornik, M. Helsen, F. Garcia-Sanchez, and B. Van Waeyenberge, "The design and verification of mumax3," AIP Advances, vol. 4, no. 10, p. 107133, 2014. [Online]. Available: http://scitation.aip.org/content/ aip/journal/adva/4/10/10.1063/1.4899186
- K. Wagner, L. Körber, S. Stienen, J. Lindner, M. Farle, and A. Kákay, "Numerical ferromagnetic resonance experiments in nanosized elements," *IEEE Magnetics Letters*, vol. 12, pp. 1–5, 2021.

Table 1. Fitted demag factors for stadium-shaped nanoislands of different aspect ratios.

Width	Length					
	\mathcal{N} vector	25 nm	50 nm	100 nm	150 nm	199 nm
25 nm	\mathcal{N}_x	0				
	\mathcal{N}_y	0				
	\mathcal{N}_z	1				
50 nm	\mathcal{N}_x	0.09156 ± 0.0491	0			
	\mathcal{N}_y	0.15480 ± 0.0491	0			
	\mathcal{N}_z	0.75365 ± 0.0491	1			
100 nm	\mathcal{N}_x	0.07330 ± 0.0665	0.08046 ± 0.0547	0		
	\mathcal{N}_y	0.13783 ± 0.0665	0.05764 ± 0.0547	0		
	\mathcal{N}_z	0.78888 ± 0.0665	0.86191 ± 0.0547	1		
150 nm	\mathcal{N}_x	0.00130 ± 0.0362	0.00529 ± 0.0243	0.01610 ± 0.0259	0	
	\mathcal{N}_y	0.20720 ± 0.0362	0.11980 ± 0.0243	0.06167 ± 0.0259	0	
	\mathcal{N}_z	0.79645 ± 0.0362	0.87491 ± 0.0243	0.92223 ± 0.0259	1	
200 nm	\mathcal{N}_x	0.00151 ± 0.0217	0.01107 ± 0.0918	0.01161 ± 0.0415	0.02146 ± 0.1139	0.01829 ± 0.20
	\mathcal{N}_y	0.19894 ± 0.0217	0.15779 ± 0.0918	0.05767 ± 0.0415	0.03214 ± 0.1139	0.02795 ± 0.26
	\mathcal{N}_z	0.79955 ± 0.0217	0.83114 ± 0.0918	0.93072 ± 0.0415	0.94662 ± 0.1139	0.95375 ± 0.20